Solid Freeform Fabrication 2021: Proceedings of the 32nd Annual International Solid Freeform Fabrication Symposium – An Additive Manufacturing Conference
Reviewed Paper

Creating Conformable Lithium Batteries Using Selective Laser Sintering

T. Phillips[1], C. Milroy[2], J. Beaman[1]

[1]Department of Mechanical Engineering, University of Texas at Austin, TX 78712
[2]Texas Research Institute Austin, TX 78746

Abstract

Selective laser sintering is an additive manufacturing technique that uses a laser to consolidate powdered material and create complex three dimensional parts. Typically, SLS utilizes thermoplastic polymer media to create dense plastic components (direct SLS). It is also possible, however, to use composite powders with non-melting additives paired with a suitable binder to create highly functional materials (indirect SLS). This paper will describe the formulation of composite materials containing conductive and electroactive material additives to fabricate lithium-ion battery components (i.e. anodes, cathodes, separators, and cases). Selective laser sintering adds to the geometric flexibility of the lithium battery components and enables batteries that conform to their surroundings, effectively reducing their geometric footprint. Preliminary galvanostatic charge/discharge test results will be presented for the functional Li-ion cathodes created using SLS, as well as next steps to improve capacity and reliability.

Introduction

The commercialization of lithium-ion (Li-ion) batteries in 1991 enabled the proliferation of miniaturized and mobile technology [1]. The high energy density, discharge rate, and lifetime have made Li-ion batteries the preferred method of energy storage for high-tech applications. Although rechargeable Li-ion batteries have powered mobile computing and telecommunications for decades, advances in energy-materials research has lagged behind global energy consumption and advances in microelectronics. As progress in improving the energy-density of insertion-compound-based electrodes has stalled, interest in "Beyond Lithium-ion" materials has increased.

A frequently-overlooked opportunity to improve energy-density lies in the opportunity to optimize the form-factor of the battery to more efficiently integrate with devices to minimize footprint and reduce overall packaging needs. By designing batteries for specific applications, the battery geometries can be tailored to fit around other components to reduce empty space and achieve greater energy storage without increasing device footprint.

Additive manufacturing (AM) is a rapidly growing field for manufacturing complex parts with little-to-no tooling, making it an ideal technology for producing on-demand batteries with an improved footprint. One of the challenges to incorporating AM in battery manufacturing is the materials restrictions often faced by AM systems [2]. Li-ion batteries incorporate diverse metals (aluminum, copper, steel), inorganic energy-storage materials, and organic compounds (polymers, conductive carbons) that must act in synergy to create a functional energy-storage device. Due to the high cost of AM equipment and material limitations, most published research efforts focus on a single battery component, typically active materials in the form of paste or slurry [3] [4].

Laser powder bed fusion (LPBF) has not been widely explored as a battery-making technology, yet offers diverse material options covering the materials needed for manufacturing of an entire battery; albeit with different machines within the LPBF family for building metal and polymer-based materials. LPBF as a battery manufacturing process introduces numerous advantages over traditional manufacturing techniques, such as facilitating creation of all battery components to create a truly conformable Li-ion battery, and substantially increasing the energy density by eliminating the current collector. LPBF also presents some advantages over other AM techniques, such as the large build volume capable of creating nested and free-floating components, resulting in increased manufacturing speed [5].

This paper will discuss progress on using indirect selective laser sintering (SLS) to create lithium battery components, with a focus on cathodes. Indirect SLS utilizes a multi-component feedstock, often with one melting component and one or more non-melting components [6]. The melting component acts as a binder for the non-melting components and post-processing steps must be taken to achieve the final desired material properties. In the work presented in this paper, a novolac phenolic resin powder was used as the melting component, which was subsequently crosslinked and pyrolyzed. Multiple material compositions have been studied and preliminary charge and discharge data will be presented for one such composition. To iterate material compositions more quickly, reduce wasted material, and optimize electrode performance, only planar, single-layer electrodes were considered.

Lithium Ion Batteries

To understand the challenges of using AM to produce batteries, the basics of Li-ion battery (LiB) operation must be understood. A lithium ion battery provides controlled electrochemical energy storage and release through the cooperative functionality of 6 major material components: cathode, anode, separator, electrolyte, current collector, and case. In commercial LiB, the anode and cathode are based on insertion materials that intercalate lithium ions. The LiB anode, or negative electrode, contains graphite, which has a very low thermodynamic reduction potential (E^o) close to that of lithium metal. The graphite hosts lithium ions between its layered sheets when the battery is in the charged state. In contrast, the cathode, or positive electrode, contains electrochemically active material(s) with a high thermodynamic reduction potential, typically in the form of a lithiated transition metal (Mn, Fe, Co, Ni) oxide or phosphate. The difference between the thermodynamic reduction potentials of the anode and cathode determines the operational voltage of the battery, and causes electrons to flow spontaneously ($\Delta G < 0$) from anode to cathode (galvanic discharge) while lithium ions migrate from anode to cathode to compensate the electrostatic charge accumulation in the cathode from the flow of electrons. In this way, the battery can provide electrical current to an external circuit during discharge, but will later require electronic current from a power supply to recharge the battery. Unfortunately, most electroactive materials used in batteries are electronic semiconductors or insulators, so commercial LiB cathodes typically contain carbon additives to increase electrical conductivity, and a polymer binder to secure the active material and conductive carbon to a metal current collector. The electrodes are kept from touching each other with a thin polymer or ceramic separator that is electronically insulating (to prevent electrical shorting and fires) but ionically conductive (to permit the passage

of lithium ions from the anode to cathode during discharge, and from cathode to anode during charge). The components are flooded with an organic carbonate electrolyte solution containing lithium salts that facilitate lithium transfer between the electrodes. The anode and cathode are mounted on electrically-conductive current collectors that provide electrical contact between the battery and an external circuit. All these components are housed within a case that protects the components and keeps the electrolyte contained. The lithium ions shuttle from the anode to the cathode during discharge (a galvanic process), and return to the anode during charging, under an electrical load from an external charger. This reversible shuttling two insertion/intercalation materials is often referred to as the "rocking chair' operational principle.

The current process for commercial LiB manufacturing involves multiple steps in which a slurry is first prepared and then coated and pressed on to metal foils (copper for anodes, aluminum for cathodes) using large roll-to-roll scale tooling. The electrodes are subsequently cut then and rolled (for cylindrical cells) or folded (for prismatic or pouch cells), with a separator sheet between each individual anode and cathode sheet. After assembly, the cells are filled with electrolyte and sealed.

Materials and Methods

Li-ion battery cathodes were created in an SLS system (Sinterstation HiQ) using a composite material system containing phenolic, carbon fibers, graphite, and lithium iron phosphate (LFP). The carbon fibers (Zoltek PX-30) had a mean length of 100 μm and width of 7 μm and composed 36.9 weight percent of the mixture. The LFP (MSE Supplies) had a mean particle diameter of 1.5 μm and composed 43.1 weight percent of the mixture. The graphite (Imerys C-nergy SFG 15L) had a mean particle diameter of 8.8 μm and composed 5 weight percent of the mixture. The remaining 15 weight percent consisted of cryo-milled phenolic (Georgia Pacific 5520). Electrodes were 12 mm diameter circles whose thickness was controlled by the laser melt penetration.

Electrode processing in the Sinterstation used a nitrogen atmosphere with less than 0.1 % oxygen and a preheat temperature of 65 ºC. Laser power was set to 20 watts and scanned at the standard speed, presumably 10,160 mm/s. Because of the large quantity of material required for a multilayer build in the Sinterstation, a pseudo multilayer technique was adopted. A thick layer (approximately 5 mm) of powder was spread, and the electrode cross sections were rescanned multiple times. Each successive scan reheats the electrode cross section and increases the depth of penetration. Forty scans were needed to penetrate deep enough into the powder bed to create an electrode with suitable strength and thickness. Successive scan lines (hatch spacing) were spaced 0.254 mm apart.

After removal from the SLS system, cathodes were crosslinked and pyrolyzed (thermally decomposed). Crosslinking was performed by placing electrodes in a preheated oven at 175 °C for 2 hours. Preheating the oven allowed the phenolic to quickly reach crosslinking temp, minimizing the amount of polymer reflow and geometric distortion experienced by the electrodes. After crosslinking, the electrodes were pyrolyzed in a vacuum furnace at approximately 300 mTorr. The temperature was ramped at 3 ºC/min to 800 °C and held for 4 hours before cooling naturally.

Scanning electron microscopy (SEM) and X-ray diffraction (XRD) were used to characterize the electrodes at different stages of post-processing.

Electrodes were stored in vacuum desiccators between each processing step and prior to electrochemical testing. Galvanostatic charge-discharge testing was carried out in coin-cell format and half-cell configuration with lithium metal foil anodes, Celgard 2500 polypropylene separators, nickel-foam spacers, and an electrolyte comprising lithium hexafluorophosphate dissolved in ethylene carbonate and ethyl-methyl carbonate (1 M $LiPF_6$ in 1:1 EC:EMC).

Results

XRD spectra for the individual components (graphite, carbon fiber, phenolic, and LFP) and the resulting electrode are given in Figure 1. Spectra for all constituent materials were taken in the material's "green", or as-purchased, state while the spectrum for the final electrode was after SLS processing and crosslinking. Electrodes in the green, crosslinked, and pyrolyzed states were able to be handled but were fairly weak and would fracture if dropped onto a hard surface from a height of 50 cm.

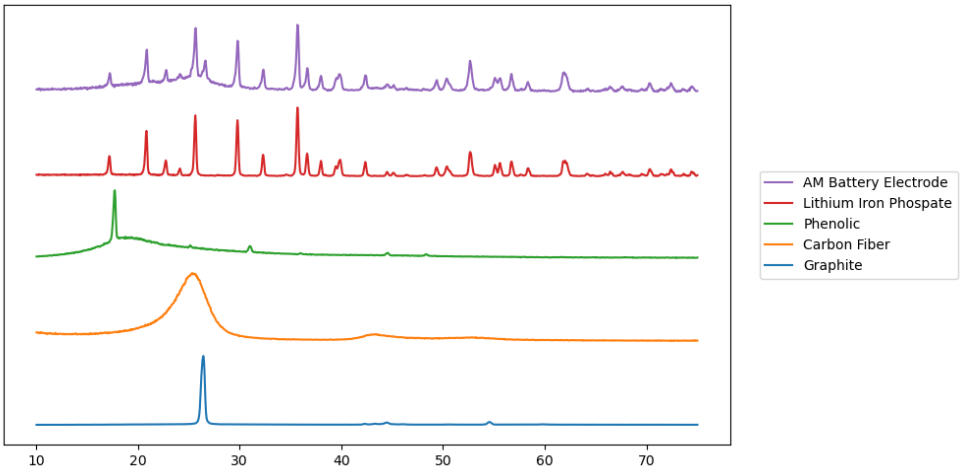

Figure 1: Normalized X-ray diffraction spectra for graphite, carbon fiber, phenolic, lithium iron phosphate, and an additively manufactured battery electrode containing all four materials.

SEM images of the raw materials used to additively manufacture a lithium-ion battery cathode are given in Figure 2 . EDS analyses are included in appendix A.

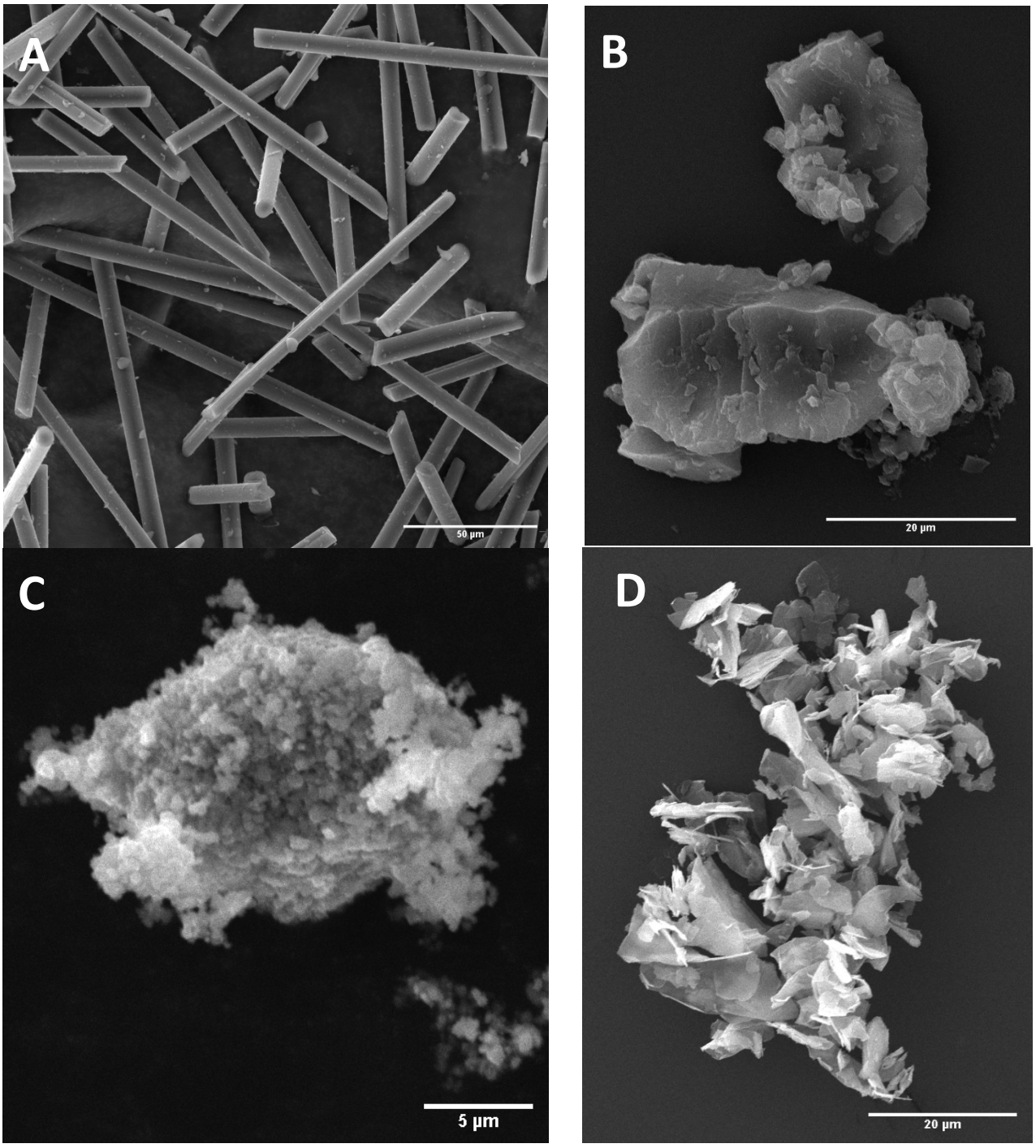

Figure 2: SEM images of battery material used for additive manufacturing of lithium batteries: (A) Carbon fibers, (B) Cryo-milled phenolic powder, (C) Lithium iron phosphate, and (D) Graphite

SEM of the as-built electrode shows significant agglomeration of LFP and material heterogeneity. Figure 3 offers images of a crosslinked cathode at different magnifications. In Figure 3(A) cracks can be seen throughout the electrode, contributing to its poor mechanical strength. Material heterogeneity can also be seen, as evidenced by the large portions or phenolic-rich material at the center of Figure 3(B) surrounded by LFP-rich regions. LFP agglomerates can

be clearly seen in Figure 3(C). It is suspected that the poor electrical contact between LFP particles impedes electrical or ionic transport to the interior particles of the agglomerates and the poor distribution of phenolic binder leads to weaker electrodes that have a decreased lifespan than those produced using traditional techniques. Energy-dispersive X-ray spectroscopy (EDS) analysis of a pyrolyzed cathode is given in Figure 4, showing the distribution of material in the electrode.

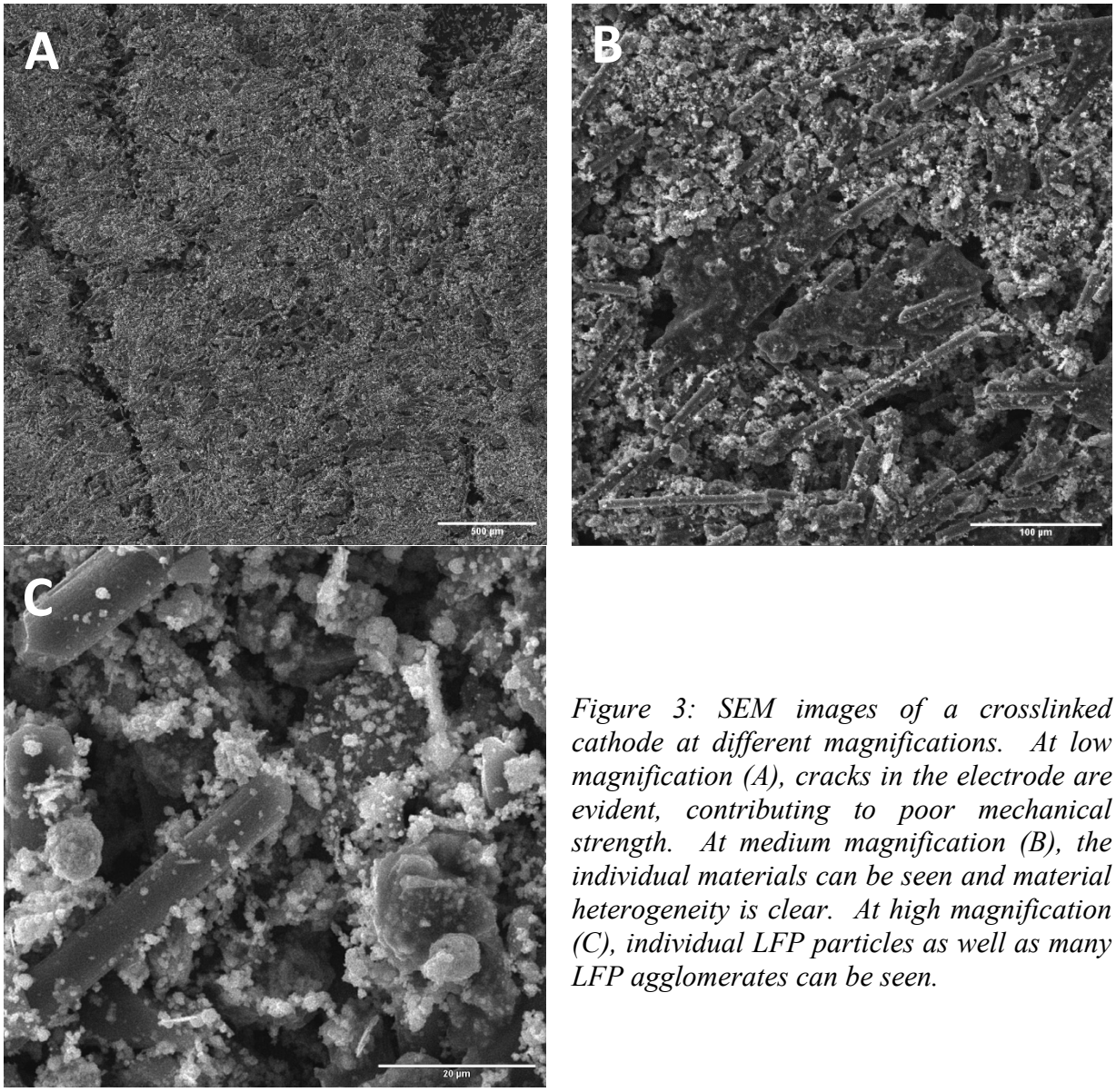

Figure 3: SEM images of a crosslinked cathode at different magnifications. At low magnification (A), cracks in the electrode are evident, contributing to poor mechanical strength. At medium magnification (B), the individual materials can be seen and material heterogeneity is clear. At high magnification (C), individual LFP particles as well as many LFP agglomerates can be seen.

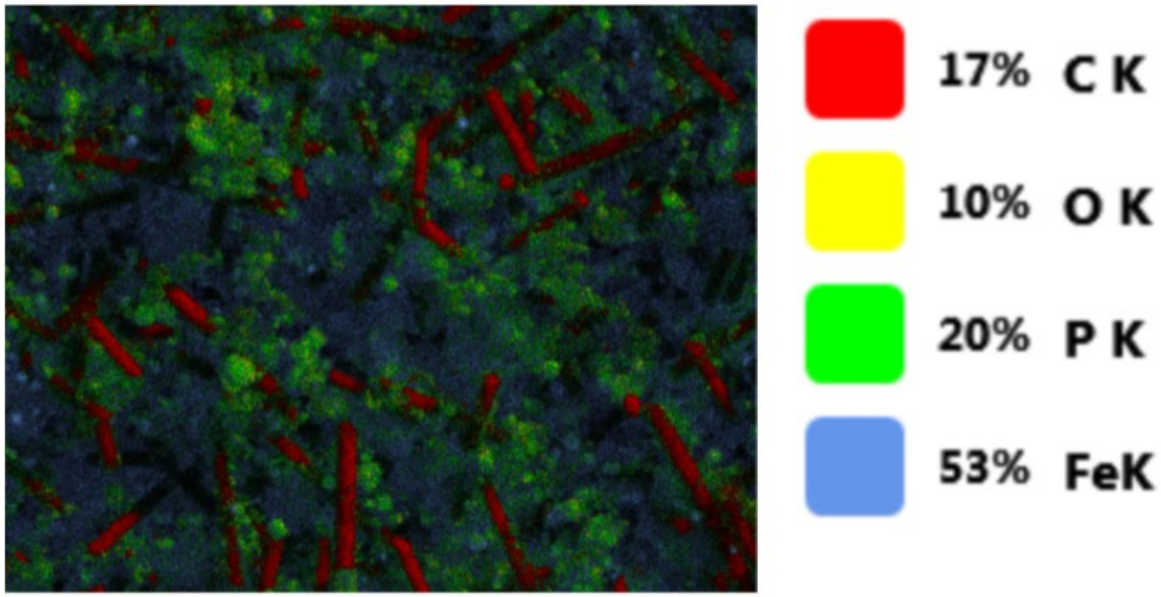

Figure 4: EDS analysis of pyrolyzed electrode showing the material distribution.

Figure 5 presents a representative plot of extended galvanostatic charge-discharge cycling of a lithium iron phosphate (LFP) cathode for one-hundred cycles at C/10 discharge rate. The cathode initially produces nearly one-third of the theoretical capacity of LFP (170 mAh/g), and the capacity and coulombic efficiency (CE) were somewhat erratic during the first five cycles. Thereafter, cycle performance was steadier, but the cathode suffered mild yet constant capacity fade. The coulombic efficiency was initially low, which is hallmark of Li-ion cells during formation of the solid-electrolyte interface (SEI) that is essential for stable long-term cycle performance. Although the CE remained above 98% after cycle ~ 12, it was still lower than a typical commercial LiB.

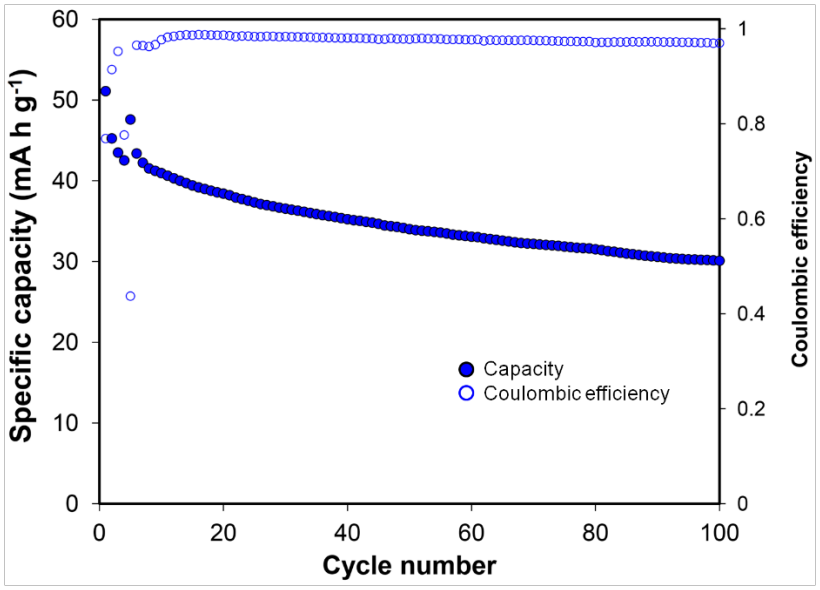

Figure 5: Extended galvanostatic charge/discharge testing of a cathode produced via additive manufacturing.

Conclusion and Discussion

Indirect selective laser sintering using phenolic binder was evaluated for manufacturing Lithium-ion battery electrodes. Cathodes containing Lithium iron phosphate, carbon fibers, graphite, and phenolic were additively manufactured and post-processed using a high-temperature vacuum furnace. Half-cell testing showed the cathode had nearly one third the theoretical capacity of LFP but experienced significant capacity fade through the first 100 cycles. While underperforming compared with traditionally manufactured lithium-ion batteries, additive manufacturing provides manufacturing flexibility that can enable on-demand manufacturing of application-specific batteries.

The results presented in this paper indicate indirect SLS is a viable method of manufacturing Li-ion battery components. Continuing work will focus on improving energy capacity and lifecycle of the electrodes. SEM analysis revealed a high amount of agglomeration and heterogeneity in the powder feedstock, both of which can contribute to decreased battery performance. Ball milling techniques will be explored to break up agglomerates and make the LFP material more electrically available. Additional mixing methods will be explored to improve the homogeneity of the material mixture to better distribute the phenolic binder.

An additional path of interest for future work is to evaluate phenolic's role in the battery and how it is affected by post-processing. Phenolic is a suitable binder in this system due to it being a high-ash polymer, converting to conductive carbon upon pyrolysis. Other researchers have found that the conversion and conductivity is influenced by pyrolysis time, temperature, and vacuum level [7] [8] [9]. Adjusting the post-processing steps to maximize electrical conductivity while maintaining structural integrity could improve the battery performance of AM electrodes.

Funding

This project is supported by Phase II funding from NAVAIR STTR topic N18A-T008 (Additive Manufacturing for Naval Aircraft Battery Applications), Contract number N68335-19-C-0578. The authors gratefully acknowledge Dr. Adam Jolley and Michael Melnick (technical points of contact at NAVAIR) for their guidance and support.

Works Cited

[1] J. T. Warner, Lithium-Ion Battery Chemistries: A Primer, Elseview, 2019.

[2] D. Bourell, J. P. Kruth, M. Leu, G. Levy, D. Rosen, A. M. Beese and A. Clare, "Materials for additive manufacturing," *CIRL Annals,* vol. 66, no. 2, pp. 659-681, 2017.

[3] Y. Pang, Y. Cao, Y. Chu, M. Liu, K. Snyder, D. MacKenzie and C. Cao, "Additive Manufacturing of Batteries," *Advanced Functional Materials,* 2019.

[4] C. L. Cobb and C. C. Ho, "Additive Manufacturing: Rethinking Battery Design," *Electrochemical Society Interface,* vol. 25, no. 75, 2016.

[5] I. Gibson, D. Rosen and B. Stucker, Additive Manufacturing Technologies: 3D Printing, Rapid Prototyping, and Direct Digital Manufacturing, New York: Springer, 2015.

[6] K. Shahzad, J. Deckers, S. Boury, B. Neirinck, J. P. Kruth and J. Vleugels, "Preparation and indirect selective laser sintering of alumina/PA microspheres," *Ceramics International,* vol. 38, no. 2, pp. 1241-1247, 2012.

[7] G. Bhatia, R. K. Aggarwal, M. Malik and O. P. Bahl, "Conversion of phenol formaldehyde resin to glass-like carbon," *Journal of Materials Science,* 1984.

[8] K. Alayavalli and D. Bourell, "Fabrication of modified graphite bipolar plates by indirect selective laser sintering (SLS) for direct methanol fuel cells," *Rapid Prototyping,* vol. 16, no. 4, pp. 268-274, 2010.

[9] S. Chen, J. Murphy, J. Herlehy, D. Bourell and K. Wood, "Development of SLS fuel cell current collectors," *Rapid Prototyping,* vol. 12, no. 5, pp. 275-282, 2006.

Appendix A: EDS Analysis

Carbon Fiber

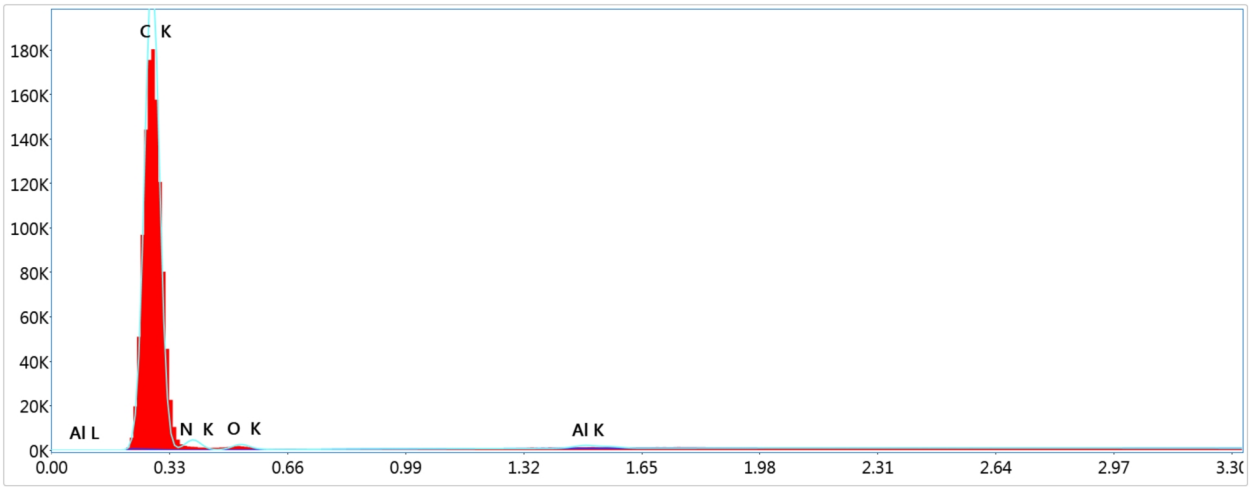

Lithium iron phosphate

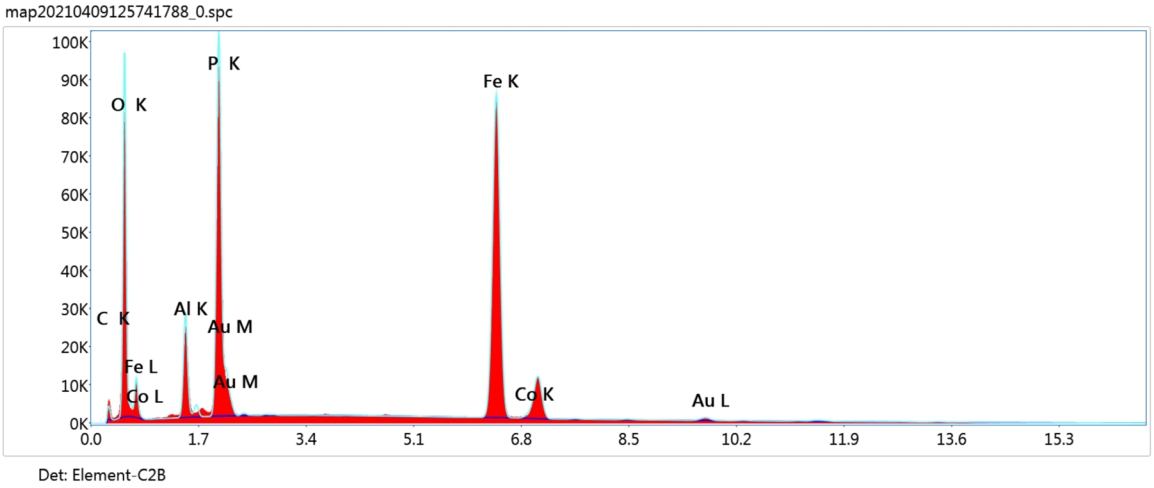

Element	Weight %	Atomic %	Net Int.	Error %	R	A	F
C K	7.09	12.28	31.96	12.54	0.8837	0.0105	1.0000
O K	49.62	64.53	1062.50	10.49	0.8951	0.0387	1.0000
AlK	6.15	4.74	398.32	9.82	0.9162	0.1252	1.0082
P K	16.45	11.05	1660.80	8.28	0.9233	0.2645	1.0078
FeK	19.25	7.17	2290.98	2.28	0.9538	0.9037	1.0463
CoK	0.30	0.11	32.40	7.40	0.9562	0.9126	1.0575
AuL	1.15	0.12	27.01	12.09	0.9736	0.9457	1.0343

Phenolic

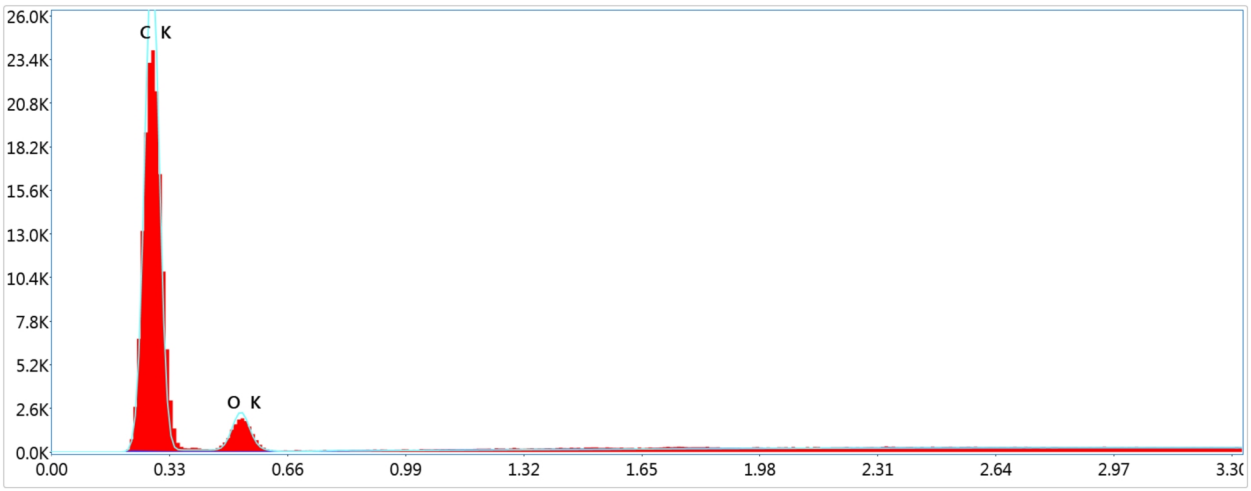

Det: Element-C2B

Element	Weight %	Atomic %	Net Int.	Error %	R	A	F
C K	86.49	89.50	307.89	7.24	0.9524	0.6618	1.0000
O K	13.51	10.50	25.91	12.86	0.9617	0.3355	1.0000

AM Electrode

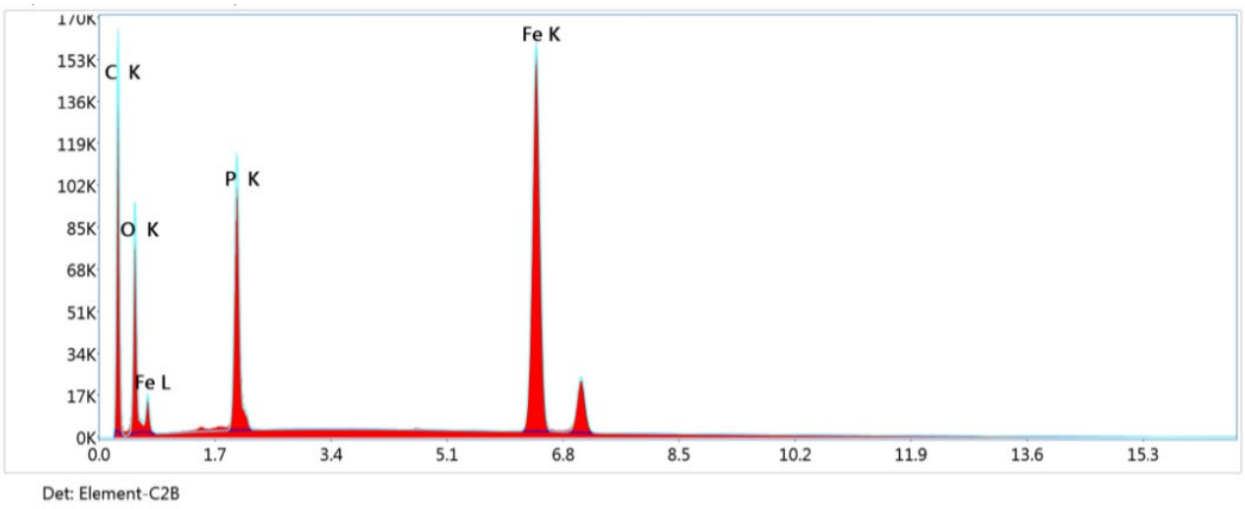

Smart Quant Results

Element	Weight %	Atomic %	Net Int.	Error %	R	A	F
C K	52.77	65.33	676.70	10.62	0.9174	0.0229	1.0000
O K	31.97	29.70	448.13	10.69	0.9265	0.0194	1.0000
P K	4.21	2.02	794.96	7.15	0.9482	0.3792	1.0100
FeK	11.05	2.94	1826.25	1.77	0.9706	0.9575	1.0556